

Rolling motion in moving droplets

SUMESH P THAMPI^{1,*} and RAMA GOVINDARAJAN²

¹The Rudolf Peierls Centre for Theoretical Physics, 1 Keble Road, Oxford, OX1 3NP, UK

²TIFR Centre for Interdisciplinary Sciences, Tata Institute of Fundamental Research, Hyderabad 500 075, India

*Corresponding author. E-mail: sumesh.thampi@physics.ox.ac.uk

DOI: 10.1007/s12043-015-0934-7; ePublication: 19 February 2015

Abstract. Drops moving on a substrate under the action of gravity display both rolling and sliding motions. The two limits of a thin sheet-like drop in sliding motion on a surface, and a spherical drop in roll, have been extensively studied. We are interested in intermediate shapes. We quantify the contribution of rolling motion for any intermediate shape, and recently obtained a universal curve for the amount of roll as a function of a shape parameter using hybrid lattice Boltzmann simulations. In this paper, we discuss the linear relationship which is expected between the Capillary and Bond numbers, and provide detailed confirmation by simulations. We also show that the viscosity of the surrounding medium can qualitatively affect dynamics. Our results provide an answer to a natural question of whether drops roll or slide on a surface and carry implications for various applications where rolling motion may or may not be preferred.

Keywords. Rolling and sliding drops; lattice Boltzmann; isoperimetric quotient.

PACS No. 47.55.nb

1. Introduction

A solid sphere on an inclined surface rolls down under the action of gravity. A rectangular object however is more likely to slide down. The choice of sliding vs. rolling motion is determined by the shape and weight of the body and the frictional forces at the supporting surface. On the other hand, a liquid drop of a given volume on an inclined surface can attain a variety of shapes. The static shape depends on the equilibrium contact angle, solid surface characteristics including the pinning location, interfacial tension between the substrates, gravity and plate inclination, while a moving drop has to contend in addition, with viscous and inertial stresses [1]. Moreover, the reaction forces and moments provided by the supporting surface are distributed and depend strongly on the shape, see e.g., [2,3]. These differences between a solid and a liquid make the study of the latter complex, but pose an interesting question, viz., whether a liquid drop sitting on an inclined solid surface will roll, slide, or do both.

Understanding the kinematics is not just a curiosity but has practical relevance too. For example, rolling droplets play an important role in self-cleaning devices. As they roll, they pick up and remove dirt as observed on hydrophobic surfaces [4]. Hence it is desirable to know under what situations one can maximize the rolling motion inside the drop.

Motion of a drop on solid surfaces has been investigated theoretically and experimentally and such studies have mostly concentrated on the two limiting cases of complete wetting and zero wetting. In the limit of complete wetting, the lubrication approximation of the Navier–Stokes equation has been widely used to study the dynamics of drops [5]. Drops mostly slide in this case and thus the assumption of parabolic velocity profile of lubrication approximation remain consistent, at least in the leading-order calculations. Sliding drops exhibit interesting instabilities of the receding front and have received much attention theoretically and experimentally (see e.g., [6,7]). In contrast, in case of hydrophobic surfaces, the contact angle approaches 180° . Such drops are expected to roll on an inclined surface under the action of gravity [8]. The shape of these droplets as they roll down has been studied in [9]. Scaling arguments in [10] of these rolling drops have been experimentally verified on superhydrophobic surfaces [11]. While these two limits are well studied, intermediate contact angles are studied much less. They are harder to analyse as they do not lend themselves to simplifying approximations. While analytical solutions are practically impossible, numerical solutions pose considerable challenges due to the presence of multiple length scales and the coupling between the evolving field and the interface shape [12]. In this study, the entire spectrum of shapes for two-dimensional drops, for a range of relevant non-dimensional parameters are analysed. A splitting of the motion into sliding, shear and rolling leads to a better understanding of the dynamics.

The competition between the rolling and sliding motions of droplets on hydrophobic surfaces has been investigated experimentally [13,14]. In these studies the effect of surface coating and roughness on the internal fluidity of the droplet was of primary concern. The velocity inside the droplet was obtained by particle image velocimetry, and the contribution to slip vs. to roll was evaluated for an accelerating drop on an inclined surface. Rolling motion is clearly observed in molecular dynamics [15], and lattice Boltzmann simulations [16] on cylindrical drops. However, such studies have concentrated on the total velocity of the droplet and its dependence on the driving force and the contact angle. With a somewhat different goal, we investigate in this study the motion of cylindrical drops of various contact angles on smooth surfaces, where the effect of fluid properties like density and viscosity, and also of slip are evaluated.

The idea of splitting the motion into shear and roll is standard in fluid mechanics. However, the standard splitting does not distinguish global rotation from local rotation of the fluid element. Such distinction is necessary to understand the global dynamics of a drop. So we distinguish between these, in the manner introduced by Kolar [17] in a different context. The splitting of the velocity field in a drop into slip and roll was done recently by Mognetti *et al* [18], although in a manner different from the method done here. This study is valid for drop sizes smaller than the capillary length, and so large deformations from the circular shape were not under consideration, while the present approach has no such restriction. We show that the shape, and hence the size, is very important in determining the amount of rolling inside the drop.

Movement of the contact line, by slipping or otherwise, is imperative for a moving drop unless the contact angle is exactly 180° [10]. Though the exact mechanism of contact line movement is not understood [19], it is generally believed that the macroscopic behaviour of the drop is independent of the assumptions at the contact line. However, it is clear that even a small amount of global rotation can manifest itself as tank-treading [20] near the contact line, which means that contact line behaviour is not local in nature, and must be consistent with the macroscopic motion. We demonstrate this using the diffuse interface (DI) model. Most earlier studies have concentrated on the rolling motion near the contact line [21,22] while we look at the rolling motion in the bulk of the drop. The association between the two, if any, implies the nonlocal hydrodynamic effects of the contact line movement [12].

In the following, we first look at sessile drops to understand the shapes of drops. We then briefly review the rolling and sliding motions of drops from the literature. Results from the simulations are presented next and then we end our discussion with a summary.

2. Static drops

Our main finding from the following sections is that rolling motion in a drop is dominantly determined by the shape. While inertial and viscous forces play their role in determining the shape, it is illustrative to look at the static drops where a competition between gravity and surface tension decides the shape of the drop.

In a static drop, variation in hydrostatic pressure inside a drop is balanced by a Laplace pressure arising from surface tension by the drop surface adopting a suitable curvature. For a two-dimensional drop, force balance along the vertical (y) direction therefore gives

$$\frac{\sigma}{R} + y\rho g = \sigma \left[\frac{d^2y/dx^2}{[1 + (dy/dx)^2]^{3/2}} \right], \quad (1)$$

where x is the horizontal coordinate at which y is the vertical location of the interface. The term in the square bracket on the right-hand side is the inverse of the radius of curvature at y , whereas R is the radius of curvature at $y = 0$ (tip of the drop). ρ , g and σ , respectively stand for density, gravitational constant and surface tension between drop and the surrounding fluid.

As gravity is the deforming force it is often quantified as a Bond number, $Bo = A\rho g/\sigma$, the ratio of gravity to surface tension. Here A is the area of the two-dimensional drop. As we vary the equilibrium contact angle (θ_e) or Bo the drop shape changes as shown in figure 1. We can define a shape parameter to characterize the shape of the drop which will be used at later sections. The isoperimetric quotient, q , given as

$$q = \frac{4\pi \times \text{Area}}{\text{Perimeter}^2} \quad (2)$$

describes the closeness of the geometry to the circle. It is exactly unity for a circle. The larger the deviations from the circle, the smaller and farther away it is from unity.

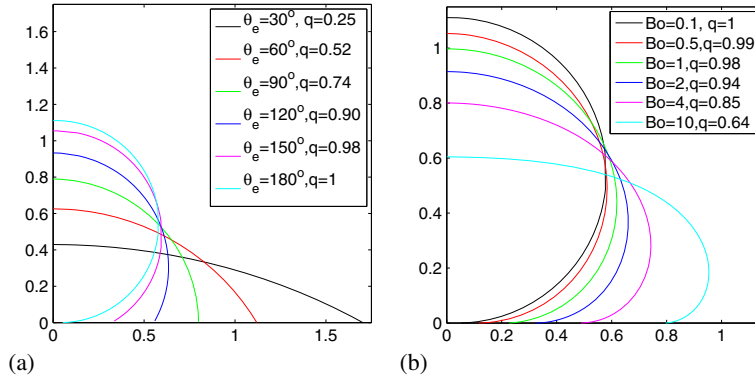


Figure 1. A balance between gravity and surface tension forces determines the shape of sessile drops. Change in the shape and hence the isoperimetric quotient are illustrated for (a) change in the contact angle (for $Bo = 0.1$) and (b) change in Bo (for $\theta_e = 180^\circ$).

3. The two limits: Rolling and sliding

Before discussing results from our simulation we briefly review the two limits which have been studied in the literature. Unlike other parts of this paper, here we consider fully three-dimensional drops.

3.1 Near-perfect rolling motion of drops

The work of Mahadevan and Pomeau [10] considered a small (drop radius $<$ capillary length) non-wetting drop under the action of a weak gravitational field ($Bo \ll 1$). Drops are assumed to be almost spherical. Assuming Huygens motion, i.e., instantaneous rotation of the drop about the point of contact, the dissipation is assumed to have occurred only near the surface. Everywhere else the motion is assumed to be the same as that of a rigid body rotation. The solid body rotation makes sense in the context of small Reynolds (Re) number flows where the energy of dissipation is expected to be minimum. Considering a balance between viscous dissipation in the layers contacting the surface and the rate of decrease of gravitational potential energy (Re is assumed to be small) the steady-state velocity of drops is obtained as

$$U \sim \frac{\sigma Bo^{-1/2} \sin \alpha}{\mu}, \tag{3}$$

where α is the plate inclination. This expression suggests that smaller drops move faster. This counterintuitive result is attributed to the fact that even though the driving force increases with increase in size, the dissipation assumed to be over the contact disk increases much more with increase in size. These calculations have been verified in [9,11] where droplet motion on superhydrophobic surfaces has been studied. The rolling motion inside such drops is evident on tracking a tracer particle as illustrated in figure 2.

Rolling motion in moving droplets



Figure 2. Trajectory of a tracer particle measured in a glycerol drop running down a superhydrophobic surface. The continuous line is a cycloid and the points are data from the experiments (adapted from [11] with permission).

3.2 Sliding motion of drops

On the other hand, sliding motion of the drops is found in the following cases: (i) if the contact angle of the drop is very small so that it forms a thin film on the surface, (ii) very large drops ($Bo \gg 1$) on hydrophobic surfaces which form puddles.

In the first case we can estimate the viscous force as $\eta U l / \theta$ where l is the radius of the solid–liquid contact area. Balancing it with gravity and in the limit of small contact angles, we get [9]

$$U \sim \alpha \frac{\rho g R^2}{\eta} \theta_c^{2/3} \quad (4)$$

suggesting a direct correlation between the driving and the dissipating forces.

In the second case, drops are larger than the capillary length and therefore the puddles have thickness twice that of the capillary length [1]. In this case, the terminal viscosity is again given by a balance between viscous dissipation in the drop and gravity. For small tilting angles ($\alpha \ll 1$), we get [9]

$$U \sim \frac{\sigma}{\eta} \alpha \quad (5)$$

suggesting that the velocity does not depend on the driving force gravity because the shape or puddle thickness is determined by gravity. As gravity changes, this thickness and hence viscous dissipation also changes making the terminal velocity independent of gravity.

4. Results and discussion

Having seen the two limits under which drops behave differently, it would be interesting to see the contribution of rolling motion in drops where none of these limits can be directly used. A detailed description of such a study can be found in [23]. We return to two-dimensional drops now. Details of theory and simulation methods are explained in Appendix A. Again taking a balance between gravity and viscous dissipation, one may obtain [6,24] the capillary number $Ca = \eta U / \sigma$ as

$$Ca \sim Bo - \Delta_\theta, \quad (6)$$

where $\Delta_\theta = \cos \theta_r - \cos \theta_a$. This quantity is generally small in our simulations. Figure 3 shows a plot of Ca vs. Bo showing the validity of the above scaling. The small deviations seen are due to inertial effects not accounted for in eq. (6), as well as by the intercept.

Rotational motion of drops on hydrophobic surfaces has been studied earlier using a diffuse interface model [18]. In this work, based on the velocity profile at the centre of the drop, drop velocity was split into a superposition of rotation and sliding. They found

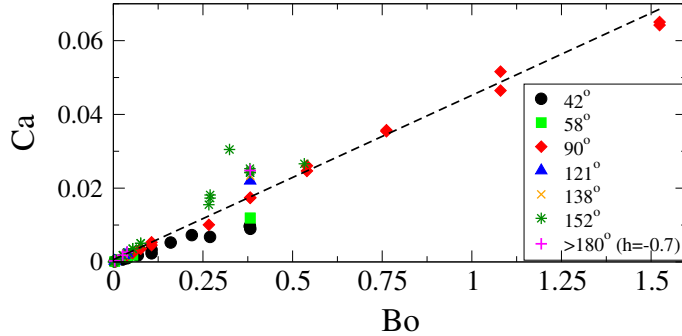


Figure 3. The linear relationship between Ca and Bo is illustrated for the data given in figure 5. These data consist of different contact angles, plate inclinations, gravity and surface tension values.

that the contribution of rolling is dependent on several parameters in the simulation. In this study we quantify rotation based on the entire area of the drop and show that it is dependent only on the geometry of the shape provided the viscosity and slip length are constant.

The steady-state drop shape and streamline patterns, total and residual vorticity and angular velocity of a drop moving on an inclined surface are illustrated in figure 4 in the centre-of-mass frame of the drop. A description about residual vorticity and the method to calculate it is explained in Appendix B. Vorticity and residual vorticity along various streamlines are also plotted as a function of azimuthal angle providing the vorticity field

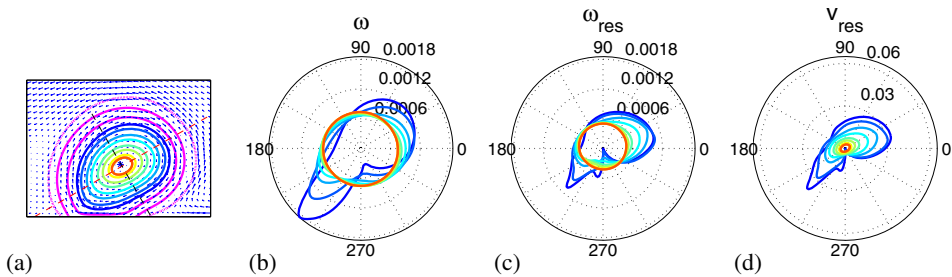


Figure 4. The shape, streamline patterns, vorticity (ω), residual vorticity (ω_{res}) and residual angular velocity (v_{res}) are illustrated for a moving drop in a coordinate frame moving with the centre of mass of the drop. A streamline of a given colour in (a) is shown in the same colour in the three polar plots of (b) ω , (c) ω_{res} and (d) v_{res} . The azimuthal angle, measured from a line parallel to the solid plate, corresponds to that of the streamline, and the radial location at a given polar angle indicates the magnitude of the respective quantities. The magenta lines represent $\psi = 0.9, 0$ and -0.9 , showing the thick interface. The drop is moving on a surface inclined to the horizontal, and the black dashed line indicates the direction of gravity. The red dashed line is normal to it. For this simulation, $Bo = 0.38$, $\%R = 28.7$, $\eta_r = 10$, $\theta_c = 152^\circ$, $Re = 124$, $Ca = 10^{-2}$.

distribution inside the drop. For a rolling solid body, the residual vorticity plot will have concentric circles. Any deviation from it shows the presence of sliding motion in the drop. Angular velocity based on residual vorticity, $v_{\text{res}} = r\omega_{\text{res}}$, where r is also plotted as a function of azimuthal angle. At small Bond number, for circular drops the streamlines look almost concentric except near the contact line. As the drop gets elongated due to larger driving force, larger deviations occur. For example, in the illustrated plot, resemblance to solid body rotation is observed only at the centre of the drop. Though deformations in the drop increases the total vorticity inside the drop, this is a result of increase in shear vorticity. Calculating residual vorticity helps to identify the right amount of rotation in such systems.

We may calculate the amount of roll, percentage rotation, denoted by $\%R$, based on the total translational velocity U of the drop, as

$$\%R = U_{\text{rolling}}/U \times 100, \tag{7}$$

where we define

$$U_{\text{rolling}} = \frac{\text{Average}(\omega_{\text{res}})}{2} \times \frac{\text{Height of the drop}}{2}. \tag{8}$$

Here the radius of the drop is taken as half of the height of the drop. It may be helpful to remember that angular velocity of a rolling solid body is half that of the constant vorticity.

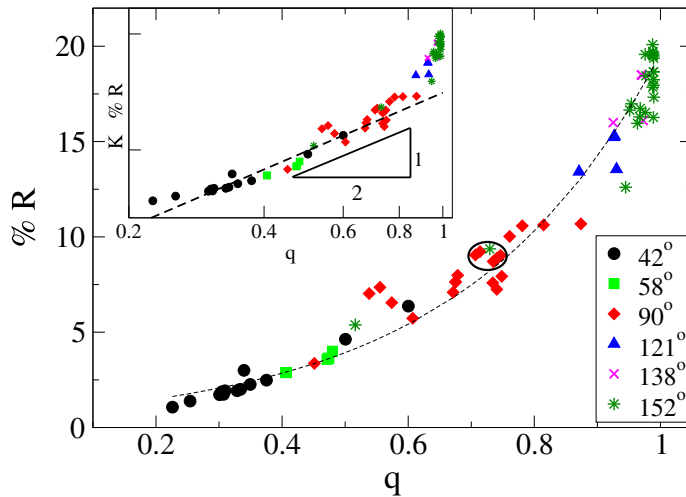


Figure 5. $\%R$ as a function of isoperimetric quotient is plotted for different sets of simulations. Each symbol represents a particular θ_e . Within each set, α varies from 4° to 176° and Bo ranges from 5×10^{-3} to 1.5. $\%R$ of drops for a wide variation in parameters fall on this curve. An exponential curve fitted through all data points is also shown. This is a universal curve giving $\%R$ as a function of shape factor for a given slip length and viscosity ratio. In the inset, the same data are plotted in log–log scale to show the consistency with scaling arguments (see text). Here, the constant, K , is chosen as 10 (adapted from [23] with permission).

An important property that determines the motion of a drop is its geometrical characteristics. Needless to say, the geometry is in turn determined by the volume, the contact angle, the gravitational force and the plate inclination, apart from the viscosity and density ratios. The effect of equilibrium contact angle is intuitive. At small contact angles any contribution of rotation to the total forward velocity is very small. As the equilibrium contact angle increases, the $\%R$ also increases. As the tilt of the plate is changed, the component of gravity parallel and perpendicular to the plate changes resulting in a variety of shapes. This has consequence on the amount of rolling in a drop. In general, the normal component of gravity decreases with increase in plate inclination from a horizontal, making the drop more circular. This helps in increasing the rolling motion. The presence of corners and deformed parts of the drop always increase the shear vorticity locally.

The isoperimetric quotient for drops is calculated from all our simulations and shown in figure 5. One may see that the $\%R$ increases as q increases to unity. However, interestingly, all data points collapse to a single curve irrespective of the equilibrium contact angle, gravity and plate inclination which determines the shape and the deformation. The viscosity ratio and mobility are kept fixed in these simulations. This universal curve gets shifted on changing the viscosity ratio or mobility in the simulations.

This universal curve can be understood from an analysis of kinematics. If the total velocity gradient, $\nabla u = \nabla u_{\text{slip}} + \nabla u_{\text{roll}}$, is denoted as a sum of slip and roll, as that resulting from two types of motion, then $\nabla u \sim U/\sqrt{A}$, where \sqrt{A} is the characteristic

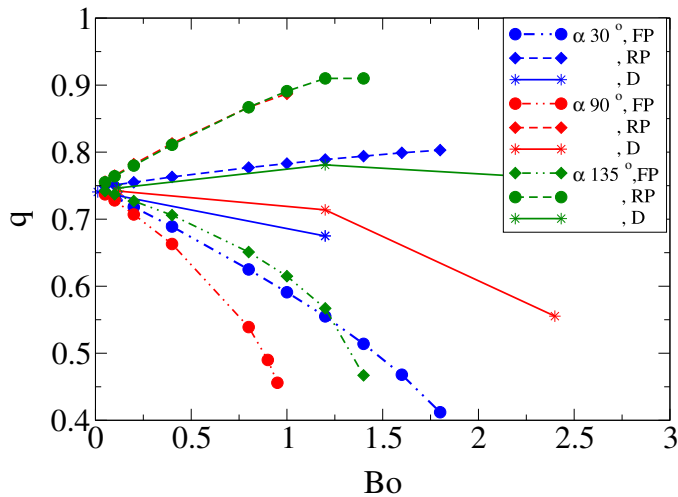


Figure 6. Isoperimetric quotient of static shapes compared with dynamic drops for the same Bond numbers. The equilibrium contact angle is 90° and three different plate inclinations, 30° , 90° and 135° , are chosen for comparison. In the figure, FP stands for front-pinned, RP stands for rear-pinned and D stands for dynamic cases. The shape factor of a dynamic drop lies in between those corresponding to front-pinned and back-pinned static shapes [2]. This behaviour breaks down at large Bond numbers where inertia is higher. In that case, the moving drop is closer to circular than either static shapes.

size of the drop, A being the area. In order to calculate the deviation of the drop from a circle, let us define two different length measures h and l , normal to, and along the solid plate, respectively. Therefore, the shape factor $q \sim A/(h + l)^2$. As $l \sim A/h$, we may represent $q \sim (h^2/A)/(1 + h^2/A)^2$ or $q = q(h/\sqrt{A})$. An estimate of the shear force, as in [10], is just $\mu U/h$ because motion is mainly parallel to the plate. Thus, $\nabla u_{\text{slip}} \sim O(U/h)$. Now ∇u_{roll} is the effective angular velocity of the drop. Then multiplying eq. (7) throughout by \sqrt{A}/U gives $\%R \sim \text{function}(q) - K$, where K is a constant resulting from exact evaluation of the above estimates. This suggests that $\%R$ is only a function of shape and this functional dependence can be completely specified in terms of isoperimetric quotient q . In the limit of small q , we can write $\sqrt{q} \sim h/\sqrt{A}$ which gives $\%R \sim \sqrt{q}$. This is shown in the inset of figure 5. For large q , i.e., when it becomes closer to a circle, the amount of roll increases more rapidly than a square root dependence would predict. It is important to mention that capillary, gravitational or wetting parameters are not used explicitly in determining $\%R$.

One may wonder whether it is possible to predict the isoperimetric quotient of the drops *a priori*. While it may not be possible to exactly calculate this, a method is provided

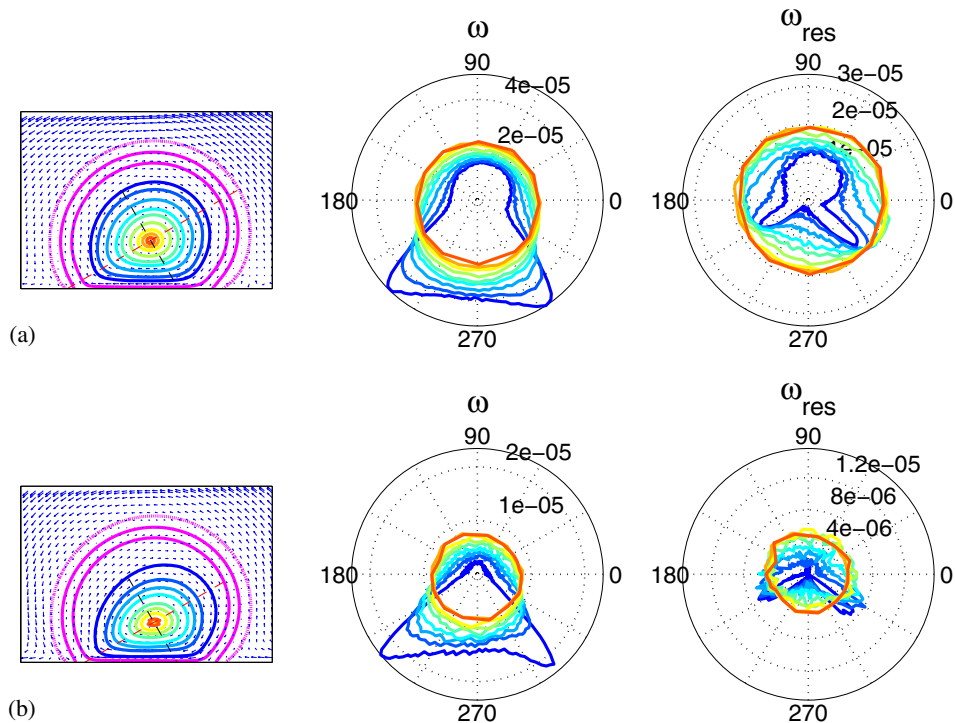


Figure 7. Change in the velocity and vorticity fields when the external fluid viscosity is changed keeping the drop viscosity the same. Here $\alpha = 30^\circ$ and $\theta_e = 138^\circ$. As the external viscosity increases, it start affecting the dynamics more. (a) $Bo = 0.19$, $\eta_r = 20$, $\%R = 22.0$, $Re = 0.3$, $Ca = 0.01$, (b) $Bo = 0.19$, $\eta_r = 1$, $\%R = 12.1$, $Re = 0.1$, $Ca = 0.004$.

subsequently to obtain an idea about it. We show in figure 6 that this can be done by analysing the corresponding static drops pinned on inclined surfaces. Minimum energy shapes of static drops can be very different based on the location of pinning [2]. We obtain these shapes with either the front end or the rear end pinned. The isoperimetric quotient of the dynamic drops stays between that of front-pinned and back-pinned drops in most of the cases for small Bond numbers. Such predictions are not correct as Bo increases and one may have carry out a full calculation of the shape to understand the dynamics of moving drops.

It must be mentioned that slip at the solid surface helps in the sliding motion of the drop and reduces the amount of roll. Our simulations in which change in mobility or viscosity changes the slip length are consistent with these expectations. The universal curve gets shifted accordingly. At very small slip lengths, very large $\%R$ is observed. Similarly, another important factor that may determine the amount of roll is the viscosity of the surrounding medium. Our simulations show that as the ratio of viscosity of the drop to that of the surroundings increases (such as in air–water) the percentage roll also increases considerably. The changes in the vorticity and residual vorticity fields as a response to change in the viscosity ratio are illustrated in figure 7. One may observe that, despite the geometry remaining similar, the $\%R$ increases when the viscosity ratio increases.

We summarize that the drop shape, expressed in terms of the isoperimetric quotient, uniquely determines the amount of rolling motion in a moving drop on an inclined surface. The amount to roll can be calculated based on residual vorticity in the flow field. Gravity and surface tension parameters do not appear explicitly, as isoperimetric quotient takes care of these competing forces by describing a shape.

Acknowledgements

The authors thank Ronojoy Adhikari and Ignacio Pagonabarraga for fruitful discussions.

Appendix A. Theory: Diffuse interface model and hydrodynamics

We use a coupled system of equations describing the hydrodynamics of a conserved order parameter ψ described by a Cahn–Hilliard equation (CHE) and the conserved momentum density $\rho\mathbf{u}$, where ρ and \mathbf{u} are the total density and local fluid velocity described by Navier–Stokes equation (NSE) [25] with additional stress densities arising from the order parameter. The order parameter evolution includes advection by fluid flow and relaxation due to chemical potential gradients. For an incompressible fluid, the dynamics is governed by

$$\partial_t \psi + \nabla \cdot (\mathbf{u}\psi) = \nabla \cdot (M\nabla\mu), \quad (\text{A1})$$

$$\partial_t(\rho\mathbf{u}) + \nabla \cdot (\rho\mathbf{u}\mathbf{u}) = -\nabla p + \eta\nabla^2\mathbf{u} + \psi\nabla\mu + \mathbf{G}. \quad (\text{A2})$$

The mobility M is the mobility relating diffusion of order parameter to the driving force $\nabla\mu$. In the above, p stands for the pressure, η is the shear viscosity and \mathbf{G} is the gravitational force density.

For a binary fluid system, the order parameter is defined as the normalized density difference and quantifies the local composition. The equilibrium thermodynamics of the fluid is described by the Landau free-energy functional [26,27]

$$F(\psi) = \int \left(f(\psi) + \frac{K}{2} |\nabla\psi|^2 \right) d\mathbf{r} + \int f(\psi_s) ds, \quad (\text{A3})$$

where \mathbf{r} stands for the spatial dimensions. The first term in the first integral represents the local free-energy density of the bulk fluid, and is approximated as

$$f(\psi) = \frac{A}{2} \psi^2 + \frac{B}{4} \psi^4$$

with $A < 0$ and $B > 0$. The three parameters A , B and K control the interfacial thickness and interfacial energy of the mixture. The second term of eq. (A3) involving the square gradient gives a free energy cost to any variation in the order parameter, and is related to the interfacial tension between the two fluid phases [28]. The last term represents the energy of interaction with walls and ψ_s is the value of order parameter at the wall. The form $f_s = H\psi_s$ is known to be sufficient to produce various wetting behaviour [29,30]. Two uniform solutions $\psi = \pm\sqrt{A/B}$ can coexist across a fluid interface. For a planar interface, the concentration profile between the two bulk phases is given by

$$\psi(z) = \sqrt{\frac{A}{B}} \tanh \frac{z}{\xi},$$

where z is the coordinate normal to the interface while $\xi = \sqrt{2K/A}$ determines the interfacial thickness. The energy associated with this profile in excess of the energy in the bulk, defined per unit area, provides the interfacial tension $\sigma = \frac{2}{3}\sqrt{2KA^3/B^2}$. The corresponding chemical potential is given by the variational derivative of the free energy with respect to the order parameter

$$\mu = \delta F / \delta \psi = A\psi + B\psi^3 - K\nabla^2\psi.$$

Gradients in the order parameter produce additional stresses, which follow from the relation $\psi\nabla\mu = \nabla \cdot \sigma^\psi$ [31], including Laplace and Marangoni stresses due to a fluid–fluid interface.

The D3Q15 lattice Boltzmann method is used for solving NSE while the method of lines with finite volume for spatial derivatives and Runge–Kutta algorithm for time integration is used for CHE. The interested reader is referred to [32] for a detailed description.

A box of $512 \times 256 \times 1$ LB units dimension are chosen for simulations. Wall boundary conditions are applied on two sides of the box and simulation was initiated with a drop of radius 60 placed on one wall and inclined at an angle to the horizontal. Simulation was continued till the drop reaches a steady-state terminal velocity.

Appendix B. Measure of rotation

We briefly discuss how the slide, shear and roll may be estimated from the flow profile. Given a velocity field in two dimensions, \mathbf{u} , the velocity gradient tensor is a 2×2 matrix

$$\begin{pmatrix} u_x & u_y \\ v_x & v_y \end{pmatrix} = \begin{pmatrix} u_x & \frac{u_y + v_x}{2} \\ \frac{u_y + v_x}{2} & v_y \end{pmatrix} + \begin{pmatrix} 0 & \frac{u_y - v_x}{2} \\ \frac{v_x - u_y}{2} & 0 \end{pmatrix}. \quad (\text{B1})$$

The symmetric part can be diagonalized to give $\begin{pmatrix} s/2 & 0 \\ 0 & -s/2 \end{pmatrix}$, where $s = \sqrt{4u_x^2 + (u_y + v_x)^2}$. This is the strain rate tensor in the principal coordinates, which represents the total straining of the fluid element. The rotation tensor, being antisymmetric, will not change with rotation of the coordinate system, and remains as $\begin{pmatrix} 0 & -\omega/2 \\ \omega/2 & 0 \end{pmatrix}$, where $\omega = v_x - u_y$, the vorticity. Therefore, in the principal axis coordinates, the velocity gradient tensor is, $\begin{pmatrix} s/2 & -\omega/2 \\ \omega/2 & -s/2 \end{pmatrix}$. The residual vorticity and strain may be written, respectively as

$$\begin{aligned} \omega_{\text{res}} &= 0 & \text{if } |s| \geq |\omega| \\ &= \text{sgn}(\omega) [|\omega| - |s|] & \text{if } |s| \leq |\omega|, \\ s_{\text{res}} &= \text{sgn}(s) [|s| - |\omega|] & \text{if } |s| \geq |\omega| \\ &= 0 & \text{if } |s| \leq |\omega|. \end{aligned}$$

We may now see that for the simple shear flow discussed above, $|s| = |\omega|$ and $\omega_{\text{res}} = 0$, while for a solid body rotation, $\omega = \omega_{\text{res}}$. If $|s| < |\omega|$, the flow is vorticity-dominated, and the residual tensor will consist of only rotation, and vice versa. Therefore, residual vorticity can characterize the rolling motion inside a drop.

By splitting the vorticity into two parts, one can identify the regions of shear. This could have also been identified by looking at the shear rate or viscous dissipation. However, such an approach will miss a very important factor to the motion which is solid body rotation which will not produce shear, but is important in determining the dynamics. Hence, looking at the actual and residual vorticity plots gives an idea about the overall motion, straining regions and rotating regions. We shall see that solid body rotation is indeed an important component in the dynamics.

References

- [1] P G de Gennes, F Brochard-Wyart and D Quere, *Capillarity and wetting phenomena: Drops, bubbles, pearls, waves* (Springer, Spring Street, New York, USA, 2004)
- [2] S P Thampi and R Govindarajan, *Phys. Rev. E* **84**, 046304 (2011)
- [3] P T Sumesh and R Govindarajan, *J. Chem. Phys.* **133**, 144707 (2010)
- [4] J P Rothstein, *Annu. Rev. Fluid Mech.* **42**, 89 (2010)
- [5] E B Dussan and R T Chow, *J. Fluid Mech.* **137**, 1 (1983)
- [6] N Le Grand, A Daerr and L Limat, *J. Fluid Mech.* **541**, 293 (2005)
- [7] J H Snoeijer, E Rio, N Le Grand and L Limat, *Phys. Fluids* **17**, 072101 (2005)
- [8] D Quéré, *Rep. Prog. Phys.* **68**, 2495 (2005)
- [9] P Aussillous and D Quéré, *J. Fluid Mech.* **512**, 133 (2004)
- [10] L Mahadevan and Y Pomeau, *Phys. Fluids* **11**, 2449 (1999)
- [11] D Richard and D Quéré, *Europhys. Lett.* **48(3)**, 286 (1999)
- [12] Y D Shikhmurzaev, *Capillary flows with forming interfaces* (Chapman & Hall/CRC, 2008)
- [13] M Sakai, J Song, N Yoshida, S Suzuki, Y Kameshima and A Nakajima, *Langmuir* **22**, 4906 (2006)
- [14] S Suzuki, A Nakajima, M Sakai, Y Sakurada, N Yoshida, A Hashimoto, Y Kameshima and K Okada, *Chem. Lett.* **37(1)**, 58 (2008)
- [15] J Servantie and M Muller, *J. Chem. Phys.* **128**, 014709 (2008)
- [16] N Moradi, F Varnik and I Steinbach, *Europhys. Lett.* **95(4)**, 44003p1 (2011)

Rolling motion in moving droplets

- [17] V Kolar, *Int. J. Heat Fluid Flow* **28**, 638 (2007)
- [18] B M Mognetti, H Kusumaatmaja and J M Yeomans, *Faraday Discuss.* **146**, 153 (2010)
- [19] D Bonn, J Eggers, J Indekeu, J Meunier and E Rolley, *Rev. Mod. Phys.* **81(2)**, 739 (2009)
- [20] E B Dussan and S H Davis, *J. Fluid Mech.* **65(1)**, 71 (1974)
- [21] A Clarke, *Chem. Eng. Sci.* **50**, 2397 (1995)
- [22] Q Chen, E Rame and S Garoff, *J. Fluid Mech.* **337**, 49 (1996)
- [23] S P Thampi, R Adhikari and R Govindarajan, *Langmuir* **29(10)**, 3339 (2013)
- [24] H Kim, H Lee and B H Kang, *J. Colloid. Interface Sci.* **247**, 372 (2001)
- [25] L D Landau and E M Lifshitz, *Fluid mechanics* (Pergamon Press, 1959)
- [26] P M Chaikin and T C Lubensky, *Principles of condensed matter physics* (Cambridge University Press, Cambridge, 1995)
- [27] J S Rowlinson and B Widom, *Molecular theory of capillarity* (Dover Publications, 1982)
- [28] V M Kendon, M E Cates, I Pagonabarraga, J C Desplat and P Bladon, *J. Fluid Mech.* **440**, 147 (2001)
- [29] J C Desplat, I Pagonabarraga and P Bladon, *Comput. Phys. Commun.* **134**, 2001 (2001)
- [30] A J Briant, P Papatzacos and J M Yeomans, *Phil. Trans. R. Soc. London A* **360**, 485 (2002)
- [31] D M Anderson, G B McFadden and A A Wheeler, *Annu. Rev. Fluid Mech.* **30**, 139 (1998)
- [32] S P Thampi, I Pagonabarraga and R Adhikari, *Phys. Rev. E* **84**, 046709 (2011)